

Universal alignment in turbulent pair dispersion

Received: 1 September 2022

Accepted: 3 July 2023

Published online: 14 July 2023

 Check for updatesRon Shnapp^{1,2}  , Stefano Brizzolara^{2,3}, Marius M. Neamtu-Halic^{2,3}, Alessandro Gambino^{2,3} & Markus Holzner^{2,4}

Countless processes in nature and industry, from rain droplet nucleation to plankton interaction in the ocean, are intimately related to turbulent fluctuations of local concentrations of advected matter. These fluctuations can be described by considering the change of the separation between particle pairs, known as pair dispersion, which is believed to obey a cubic in time growth according to Richardson's theory. Our work reveals a universal, scale-invariant alignment between the relative velocity and position vectors of dispersing particles at a mean angle that we show to be a universal constant of turbulence. We connect the value of this mean angle to Richardson's traditional theory and find agreement with data from a numerical simulation and a laboratory experiment. While the Richardson's cubic regime has been observed for small initial particle separations only, the constancy of the mean angle manifests throughout the entire inertial range of turbulence. Thus, our work reveals the universal nature of turbulent pair dispersion through a geometrical paradigm whose validity goes beyond the classical theory, and provides a framework for understanding and modeling transport and mixing processes.

If we took a handful of small passive particles and threw them into the ocean, how long would it take before the particles became fully mixed in the oceans across the globe? Answering questions like this requires that we know the rates at which turbulent flows transport and diffuse the materials that they carry. One characteristic of transport is the so-called pair dispersion, which describes the rate at which two particles separate from each other. Pair dispersion can be used to calculate the variance of the concentration fluctuations of substances carried by the flow¹, so it is of critical importance in numerous applications such as determining the rate of ozone destruction in the atmosphere² or the dispersion of pollutants in the ocean³.

In quiescent fluids particles undergo Brownian motion, so the increase of the distance between two particles is a diffusive process with constant diffusivity. However, in turbulence, particles are transported by the flow field and so the process is driven by advection. Turbulent pair dispersion is divided into three regimes (see reviews in refs. 4–6). First, at very short times, the finite fluid inertia dictates that

the relative velocity of particles remains approximately constant. This leads to the so-called "ballistic" regime, in which the inter-particle distance scales linearly with time¹. The ballistic regime occurs at times $t < \tau_b$, where $\tau_b = (l_0^2/\epsilon)^{1/3}$ is the Batchelor time scale (l_0 is the initial distance between particles and ϵ is the mean dissipation rate of kinetic energy into heat). The second, so-called "diffusive" regime of separation ensues at very long times when the inter-particle distances, l , are outside the inertial range, $l \gg L$ (where L is the integral length scale). There, similarly to the Brownian motion case, the velocity field is uncorrelated and the typical inter-particle distance grows with a square-root scaling in time⁷. The third regime was introduced by Richardson nearly a century ago⁸, and it is still intensely debated today. This regime corresponds to the inertial range of turbulence, namely, $\eta \ll l \ll L$, where $\eta = (\nu^3/\epsilon)^{1/4}$ is the Kolmogorov length scale (ν is the kinematic viscosity). In this inertial regime the typical separation velocities increase with the separation distance, which leads to a super-diffusive growth of inter-particle distances.

¹Department of Mechanical Engineering, Ben-Gurion University of the Negev, Beer-Sheva P.O.B. 653, Israel. ²Swiss Federal Institute of Forest, Snow and Landscape Research WSL, Birmensdorf 8903, Switzerland. ³Institute of Environmental Engineering, ETH Zürich, Zürich CH-8039, Switzerland. ⁴Swiss Federal Institute of Aquatic Science and Technology Eawag, Dübendorf 8600, Switzerland. ✉ e-mail: ronshnapp@gmail.com

While the validity of the ballistic and the diffusive regimes are generally agreed upon by the community, Richardson’s inertial regime remains contested. Indeed, although Richardson’s theory was proposed nearly a century ago⁸, and despite it being considered a hallmark of turbulence, it remains elusive to empirical verification. In particular, finite Reynolds number effects^{9–17}, and intermittency and mixing of different regimes^{18–20}, make it difficult to interpret the measurements of the time evolution of the statistics of interparticle distances over long periods of time. Indeed, empirical studies that measured pair dispersion scaling exponents found agreement with Richardson’s theory only for particular choices of initial conditions, namely small initial distances^{10,16,17,21,22} or separation velocities¹⁵, while for other initial conditions the scaling exponent were different. This gap between the classical theory and modern experiments demands an explanation that will better describe the process across the scales.

In this paper, we propose a new approach for characterizing turbulent pair dispersion. Specifically, we focus on the angle, θ , formed between the relative position and relative velocity vectors (see Fig. 1, and Supplementary Video 1). We show theoretically and confirm empirically that this angle has three unique behaviors in each of the three regimes of the separation process. In particular, in the inertial regime it has a constant mean value that is equal to approximately 59° independently of the initial conditions and the Reynolds number. Thus, it is a universal constant of turbulence. Furthermore, we calculate the mean value of the angle analytically using Richardson’s theory at small initial separations, finding agreement with the empirical data. Thus, our work introduces a geometrical framework that reveals the universality of turbulent pair dispersion and applies more broadly than the traditional picture. This provides a framework for characterizing dispersion in oceanic and atmospheric turbulent flows.

Results

Theoretical analysis of the pair dispersion angle

We begin by calculating theoretical predictions for the average of θ in turbulence. To elucidate our analysis, we will consider three different scenarios: first, particles that move with constant velocities, second,

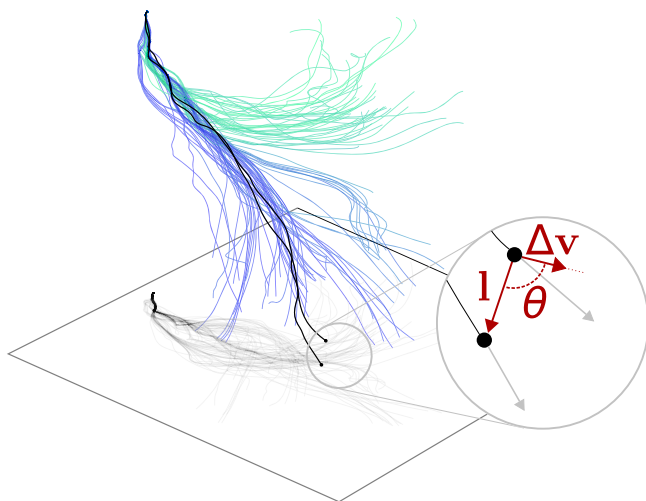


Fig. 1 | Pair dispersion angle definition. Visualization of a group of Lagrangian fluid particle trajectories in a turbulent flow, starting from within a cube with dimensions of one Kolmogorov length scale. Trajectories are color-coded according to their final position. The relative position vector, the relative velocity, and the angle between them, \mathbf{l} , $\Delta\mathbf{v}$, and θ , respectively, are shown for one particle pair. In the inertial range, the average of θ calculated over all pairs is equal to a constant value.

particles that undergo normal diffusion, and third, particles that undergo a super-diffusive separation. These three scenarios correspond to the three regimes of pair dispersion in turbulence namely, the ballistic, diffusive and inertial regimes respectively. We consider particles that have initial positions $\mathbf{x}_1(0)$ and $\mathbf{x}_2(0)$, and move with velocities, $\mathbf{v}_1(t)$ and $\mathbf{v}_2(t)$, respectively. Their relative velocity is $\Delta\mathbf{v}(t) = \mathbf{v}_1(t) - \mathbf{v}_2(t)$. The distance between them, $l(t) \equiv |\mathbf{l}(t)| = |\mathbf{x}_1(t) - \mathbf{x}_2(t)|$, follows the kinematic relation^{9,23}

$$\frac{dl}{dt} = \frac{\Delta\mathbf{v} \cdot \mathbf{l}}{l}. \tag{1}$$

The cosine of the angle that lies between the relative velocity and relative position vectors is equal to

$$\cos(\theta) \equiv \alpha = \frac{\Delta\mathbf{v} \cdot \mathbf{l}}{|\Delta\mathbf{v}|l}, \tag{2}$$

where it can take values between -1 and 1 , which correspond to θ ranging from 180° to 0° . Combining Eqs. (1) and (2) shows that

$$\alpha = \frac{1}{|\Delta\mathbf{v}|} \frac{dl}{dt}. \tag{3}$$

In the first scenario, the ballistic case, the particles’ velocities are frozen in time. Thus, the relative position in this regime evolves as $\mathbf{l}(t) = \mathbf{l}(0) + \Delta\mathbf{v}t$, and the angle cosine can be solved analytically, giving

$$\alpha(t) = \frac{\Delta\mathbf{v} \cdot (\mathbf{l}(0) + \Delta\mathbf{v}t)}{|\mathbf{l}(0) + \Delta\mathbf{v}t| |\Delta\mathbf{v}|}. \tag{4}$$

Therefore, in the ballistic scenario $\alpha(t)$ increases monotonically and tends asymptotically towards 1 for any $\mathbf{l}(0)$ and $\Delta\mathbf{v}$. Correspondingly, the two vectors tend towards perfect alignment with time, namely, $\theta \rightarrow 0^\circ$.

We move on to the second scenario by analyzing the time evolution of $\langle \alpha \rangle$ (where brackets denote an ensemble average) for an ensemble of particles that undergo diffusion with a constant diffusivity. Specifically, we consider an ensemble composed by taking pairs of particles at different locations and times with the same initial separation $\mathbf{l}(0) = \mathbf{l}_0$, while allowing them to separate with time. Initially, there is no preferred alignment ($\langle \alpha(0) \rangle = 0$) since the particles’ velocities are chosen randomly. Furthermore, the particles separate from each other on average, so $\langle \frac{dl}{dt} \rangle > 0$; together with Eq. (3), this suggests that $\langle \alpha(t) \rangle$ immediately grows and becomes positive for $t > 0$. To determine the long time behavior we transform to a frame of reference whose origin is fixed at $\mathbf{x}_1(t)$. Then, considering long times for which $l(t) \gg l_0$ (where $l_0 \equiv |\mathbf{l}(0)|$), the average distance between pairs in three dimensional space is given by $\langle l(t) \rangle = (\frac{16}{\pi} Dt)^{1/2}$, where D is the diffusivity for the relative dispersion, equal to twice the single particle diffusivity. Taking the time derivative and using Eqs. (1) and (2), we obtain the long-time scaling $\langle \alpha(t) \rangle \sim \sqrt{\frac{4D}{\pi \langle |\Delta\mathbf{v}|^2 \rangle}} t^{-1/2}$. Thus, at long times, $\langle \alpha \rangle$ decays asymptotically back towards zero with a time scaling of $t^{-1/2}$, so that $\langle \theta(t) \rangle \rightarrow 90^\circ$. The asymptotic decay in this case occurs because $\langle l \rangle$ grows with time with a scaling exponent smaller than 1 , while the statistics of $\Delta\mathbf{v}$ are constant.

Moving forward to the third scenario, pair dispersion in the inertial range of turbulence is intrinsically different from the above cases, since both the scaling of $\langle l \rangle$ is different, and statistics of $\Delta\mathbf{v}$ depend on the scale l . Indeed, a preferential oblique alignment between \mathbf{l} and $\Delta\mathbf{v}$ was observed in direct numerical simulations (DNS)^{9,19}. To calculate the mean value of α we use eq. (3) and expand it

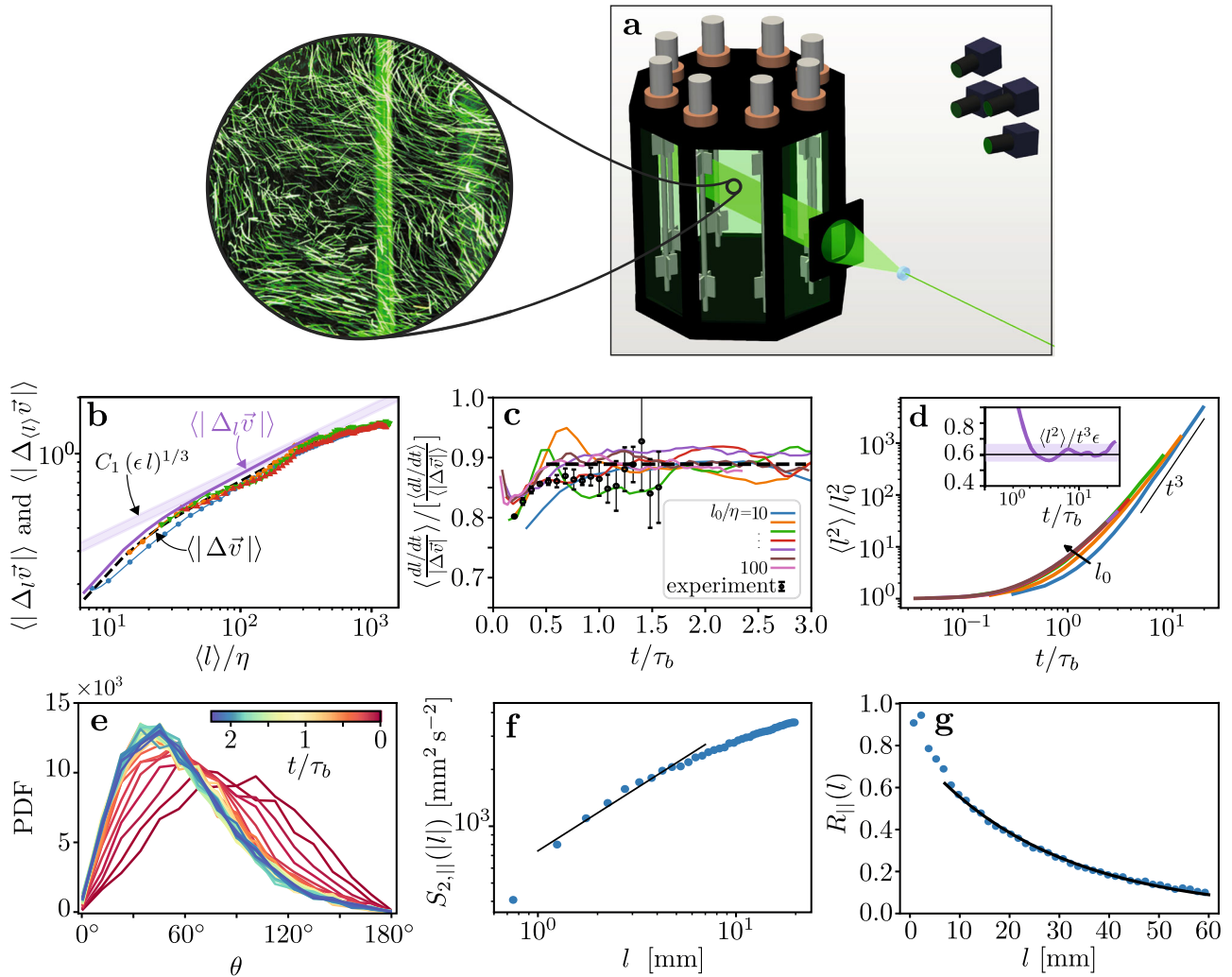


Fig. 2 | Turbulence characterization. **a** A sketch showing the experimental water tank, four camera system, laser light, and a streak image of flow tracers in the apparatus. **b** The Eulerian first-order absolute structure function is shown as a purple line, and a shaded region shows the Kolmogorov scaling with $C_1 = 2.7 \pm 0.15$. The absolute, first order, mixed Eulerian-Lagrangian structure function is shown as shapes for particle groups with $l_0/\eta = 5, 15, 25, 35 \pm 5$, and the black dashed line shows our theoretical prediction (eq. (16)). Data shown was taken from the DNS. **c** The correction factor due to the series truncation in eq. (5), plotted against time for data taken from the DNS for $l_0/\eta \in (10, 20, 30, 40, 50, 70, 100)$, and the experimental results, averaged over l_0 in the inertial range with uncertainty calculated by bootstrapping over three groups. **d** Mean squared particle separation is

plotted against time for $l_0/\eta < 5, 5 < l_0/\eta < 10, 10 < l_0/\eta < 20, 40 < l_0/\eta < 50, 60 < l_0/\eta < 70$, and $90 < l_0/\eta < 100$. The inset shows the same property for particles with $2 < l_0/\eta < 4$, normalized according to eq. (6), where $g = 0.52 \pm 0.06$ is shown as a shaded region. Data shown uses the DNS results. **e** The PDF of θ is shown at various times as indicated by the color of the curves. Data is shown for $l_0 = 50\eta$ using the DNS results. **f** The Eulerian second-order longitudinal structure function in the experimental dataset is plotted against the distance, l . The black line and shaded region show the Kolmogorov scaling range for $10\eta < l < 40\eta$. **g** The longitudinal spatial correlation function of velocity fluctuations, averaged over spherical shells of radius l in the experimental data set. The line shows an exponential fit to the tail of the data.

as a Taylor series around the mean values of $|\Delta v|$ and $\frac{dl}{dt}$. By averaging the series, we obtain the following expression for the mean value

$$\langle \alpha \rangle = \left\langle \frac{1}{|\Delta \mathbf{v}|} \frac{dl}{dt} \right\rangle = \alpha_0 \left(1 + \sum_{n=1}^{\infty} \frac{\alpha_n}{\alpha_0} \right) \quad (5)$$

where α_n is the averaged n^{th} term of the series, and $\alpha_0 = \frac{1}{\langle |\Delta \mathbf{v}| \rangle} \frac{d \langle l \rangle}{dt}$ (the derivation is given in Section 4.4). In what follows, we assume that the series converges sufficiently fast and truncate terms with $n \geq 2$. This results in a first order approximation of Eq. (5), the accuracy of which is confirmed in Section 2.2. Then, since $\alpha_1 = 0$, we obtain that $\langle \alpha \rangle = \alpha_0$.

The behavior of α_0 could first be considered from a dimensional analysis point of view. In the inertial range, Kolmogorov's local

isotropy theory leads to the conclusion that α_0 can only depend on ϵ , l_0 , and t . In addition to that, α does not depend on l explicitly but only on $\frac{dl}{dt}$ (Eq. (3)). Therefore, and because $\frac{d \langle l \rangle}{dt} = \frac{d \langle l - l_0 \rangle}{dt}$, it is reasonable to assume that α_0 is independent on l_0 in the inertial range. This leaves only ϵ and t as the parameters of the problem in the inertial range. However, no dimensionless group can be constructed from these two parameters, so to ensure dimensional homogeneity, $\langle \alpha \rangle$ has to be constant. The actual validity of this assumption is verified below (Section 2.2).

We can also calculate α_0 using Richardson's theory in the range in which it is valid. Thus, we calculate $d \langle l \rangle / dt$ and $\langle |\Delta \mathbf{v}| \rangle$ in the inertial range. When $l(t)$ is in the inertial range and sufficient time has passed such that $\langle l(t) \rangle \gg l_0$, Richardson's law predicts the following super-

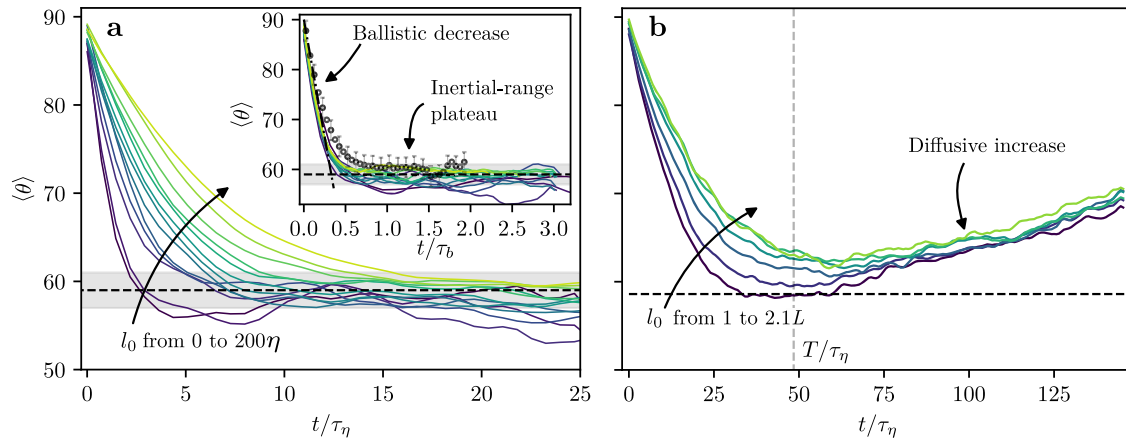


Fig. 3 | Evolution of the pair dispersion angle. **a** Evolution of the average angle between the separation and the relative velocity vectors as a function of time. Continuous lines show DNS results for various ensembles grouped by the initial separation distance for values in the inertial range; the bin edges used to form the ensembles are $l_0/\eta = 0, 10, 20, 30, 40, 50, 60, 70, 80, 90, 100, 130, 160,$ and 200 , where the arrow runs from lower to higher values. Lines in the inset show the same data plotted with time normalized by the Batchelor timescale. Circles correspond to the experimental results, averaged over all pairs with $r_0 < 70\eta$ with an uncertainty

of $\pm 2^\circ$ based on the data range across the l_0 groups (Fig. S3). The dot-dashed line correspond to eq. (9). The dashed black line and the shaded region mark the estimated value of $\langle \theta \rangle = 59.3 \pm 2^\circ$. **b** Evolution of the average of θ for pairs with initial separation outside the inertial range. Data are shown for initial separation distances of $l_0/\eta = 483, 594, 704, 812, 915,$ and 1006 . These values correspond to $l_0/L = 1.00, 1.24, 1.47, 1.69, 1.91,$ and 2.10 . The horizontal dashed line marks the $\langle \theta \rangle = 59.3^\circ$ value, and the vertical dashed line marks one integral timescale.

diffusive pair dispersion regime^{6,8}

$$\langle l^2 \rangle = g \epsilon t^3, \tag{6}$$

where g is the Richardson constant. We also make use of the fact that there are two theoretical predictions for the probability density function (PDF) of l in the inertial range^{1,6,8,13}. In both theories, the average separation is equal to $\langle l \rangle = b \sqrt{\langle l^2 \rangle}$, where $b = 0.867 \pm 0.054$ is a dimensionless constant (see Section 4.2). Combining this with Eq. (6) we obtain $\frac{d\langle l \rangle}{dt} = \frac{3}{2} b (g\epsilon t)^{1/2}$. Notably, Richardson’s solution is strictly valid only for $l_0 = 0$, and thus the variance of l in Eq. (6) is usually replaced with the variance of $(l - l_0)$ ⁶. Yet, since $\frac{d\langle l \rangle}{dt} = \frac{d\langle l - l_0 \rangle}{dt}$, and since the PDF of $l - l_0$ was experimentally observed to agree with the theoretical expressions used here for the PDF of l ^{6,13}, our calculation applies also for finite l_0 . The second factor, $\langle |\Delta \mathbf{v}| \rangle$, is the first order Eulerian-Lagrangian absolute structure function, where the relative velocities are taken over the full distribution of particle distances which changes with time. At $t = 0$, the structure function is purely Eulerian, so according to the Kolmogorov theory²⁴ (namely, neglecting intermittency corrections), $\langle |\Delta \mathbf{v}| | t = 0 \rangle = \langle |\Delta \mathbf{v}_0| \rangle = C_1 (\epsilon l_0)^{1/3}$, where C_1 is a universal constant of turbulence. At longer times, the mixed structure function is calculated by averaging the particles’ relative velocities across the distribution of particle distances, l ; in the inertial range we obtain $\langle |\Delta \mathbf{v}| \rangle = c C_1 \left(\epsilon \sqrt{\langle l^2 \rangle} \right)^{1/3}$, where $c = 0.918 \pm 0.034$ is a dimensionless constant (see Section 4.3). Combining these estimations and using Eq. (6) we obtain the following first order, mean-field approximation, for the angle cosine in the inertial range of turbulence

$$\langle \alpha \rangle = a \frac{g^{1/3}}{C_1}, \tag{7}$$

where $a \equiv \frac{3b}{2c} = 1.42 \pm 0.10$.

Equation (7) connects $\langle \alpha \rangle$ with Richardson’s law in the inertial range, and it has several important implications. First, our calculations suggest that $\langle \alpha \rangle$ in the super-diffusive regime is constant. This is in agreement with the dimensional analysis argument presented above,

which is expected as eq. (6) can also be derived from a similar argument⁴. Indeed, the value of $\langle \alpha \rangle$ obtained here does not depend on ϵ nor on the initial conditions, so it is a universal constant of turbulence. The value of $\langle \alpha \rangle$ can be calculated with eq. (7) for the small initial separations for which Richardson’s theory holds, and then, assuming that $\langle \alpha \rangle$ is independent on l_0 , the same value should hold for the entire inertial range (this is verified in Section 2.2). Second, because of the geometrical constraint $|\alpha| \leq 1$, and since all the constants in eq. (7) are positive, we obtain a constraint for the value of the Richardson constant

$$g \leq \left(\frac{C_1}{a} \right)^3. \tag{8}$$

Third, if one measures $\langle \theta \rangle$ from empirical data, the value of g can be readily calculated.

Universality of the pair dispersion angle

The angle θ can be measured from the trajectories of flow tracers, and thus, its behavior can be tested using empirical data directly. To this end, we used two independent datasets. The first is the Johns Hopkins Turbulence Database (JHTDB), which holds turbulent flow fields taken from a direct numerical simulation (DNS) of a forced homogeneous isotropic turbulence at a Taylor microscale Reynolds number of $Re_\lambda \approx 433$, with the ability to integrate Lagrangian trajectories^{25,26}. Since its publication, this database has become a gold standard and a hypothesis-testing tool for turbulent flows. The second data set was taken from 3D particle tracking measurements^{27,28} of quasi-homogeneous isotropic turbulence that we conducted inside a stirred water tank at ETH Zürich (Fig. 2a and Supplementary Video 2, the data is available in ref. 29). The flow had secondary circulation with an amplitude of about 68% of the root mean squared turbulent fluctuations. The turbulence integral length scale, $L = 20.5$ mm, was calculated by fitting an exponential function to the longitudinal velocity auto-correlation function (Fig. 2g), where a Kolmogorov scaling range was observed between approximately 1 and 5 mm for the Eulerian second order structure function (Fig. 2f). The Reynolds number was $Re_\lambda \approx 188$. Detailed information about both data sets are given in Section 4.

We begin by evaluating the error that results from truncating the Taylor series in eq. (5). The ratio between $\langle \alpha \rangle$ and its first order

approximation varies slightly with time where the same trend is observed for both data sets. At $t = 0$ it equals approximately 0.8, and it then increases with time, plateauing at approximately 0.89 for $t \geq \tau_b$ (Fig. 2c). Therefore, the error introduced by truncating the series amounts to approximately 10% of the value of $\langle \alpha \rangle$ and it does not change with time. Since the correction is constant throughout the inertial range, truncating the series does not affect the constancy predicted for $\langle \theta \rangle$. This observation might be explained by the fact that the higher order terms result from correlations between l and Δv (Section 4.4), which should not change with time in the self-similar inertial range.

Next we confirm our calculation for the first order absolute structure function. The Eulerian structure function, shown in Fig. 2b, is compared with the Kolmogorov scaling, where neglecting intermittency corrections to the scaling exponent we obtain $C_1 = 2.7 \pm 0.15$. Furthermore, plotting the mixed Eulerian-Lagrangian structure function we obtain good agreement with Eq. (16). Overall, Fig. 2b and c confirm the hypotheses made in the derivation of Eq. (7), and suggest that the error due to the Taylor series truncation is reasonably small.

We now turn to estimating the Richardson constant, g . The growth of $\langle l^2 \rangle$ as a function of time is shown in Fig. 2d for particles taken from the DNS results. As commonly observed, we can identify a range in which Eq. (6) holds only for pairs with small initial separations^{10,16,17}. Therefore, using particles with the initial separation $2\eta < l_0 < 4\eta$, we estimate $g = 0.52 \pm 0.06$ (Fig. 2d, inset), which is in good agreement with previous measurements^{6,30}. Furthermore, using the value we measured for C_1 , eq. (8) gives $g \leq 6.91$, which agrees with our measurements and with previous estimates⁶.

Next we turn to measure the pair dispersion angle for particles in the empirical data sets using Eq. (2) directly. The main panel of Fig. 3a shows the evolution of $\langle \theta \rangle$ as a function of time for twelve pair ensembles from the DNS dataset, whose initial separation distance is inside the inertial range ($\eta < l_0 < L$). For all cases, the average angle is initially very close to 90° (values slightly smaller than 90° are due to the well-known skewness of Eulerian velocity differences in turbulence⁴). Correspondingly, the PDF of θ , that ranges from 0° to 180° , is symmetrical around 90° (Fig. 2e). Indeed, since the particles are chosen randomly, there is no significant preferred alignment between \mathbf{l} and $\Delta \mathbf{v}$ at $t = 0$.

For $t > 0$, the average angle rapidly decreases until a plateau is reached where the time of convergence of $\langle \theta \rangle$ to the plateau increases with the initial separation distance. In the ballistic regime, $t \ll \tau_b$, during which $\Delta \mathbf{v}$ is constant, simple geometrical considerations show that $\theta = \frac{\pi}{2} - \frac{|\Delta_{\perp} v|}{|v_0|} t$, where $\Delta_{\perp} v$ is the transverse component of the relative velocity. Taking the average of this relation over particles with the same l_0 while using the Kolmogorov scaling of the velocity differences we obtain the solution for short times

$$\langle \theta \rangle = \frac{\pi}{2} \left(1 - \frac{t}{\tau_b} \frac{2C_{1,\perp}}{\pi} \right) \quad \text{for } t \ll \tau_b, \quad (9)$$

where $C_{1,\perp} \approx 1.66$ is the coefficient for the transverse absolute first-order structure function ($\langle |\Delta_{\perp} v| \rangle$) measured from our data. Therefore, to compensate for the differences in the convergence rate for pairs with different l_0/η , time is normalized by τ_b for the DNS and the experimental datasets. Following this normalization, the data from the DNS and from our experiment collapse, and good agreement is found with Eq. (9) (Fig. 3a inset). The plateau is reached at $t/\tau_b \geq 0.5$, approximately the time that marks the beginning of the super-diffusive regime³⁰. Since in ballistic motion $\langle \theta \rangle$ decreases monotonically, and since the transition in Fig. 3a occurs at fixed t/τ_b , we infer that the transition in the trends of $\langle \theta \rangle$ is due to the transition of pair dispersion from the ballistic to the inertial, super-diffusive regime. Therefore, the plateau observed for $\langle \theta \rangle$ in Fig. 3a occurs during the turbulent inertial regime; this confirms our prediction that $\langle \theta \rangle$ attains a constant value in

the inertial range, and that a plateau marks the inertial regime. Correspondingly, the PDF of θ becomes increasingly asymmetrical through the ballistic regime since its mode shifts to the left; eventually it reaches a steady-state for $t/\tau_b \geq 0.5$, namely in the inertial range (Fig. 2e).

The value of the plateau of $\langle \theta \rangle$ does not show a systematic dependence on l_0 nor on ϵ , which is in accordance with the assumption presented in Section 2.1 and with Eq. (7). In particular, the difference between the plateaus observed in the DNS and the experimental data is smaller than 2° (58.6° in the DNS and 60.3° in the experiment), which is comparable to our uncertainty levels. This observation supports our prediction that the value of $\langle \theta \rangle$ (and $\langle \alpha \rangle$) in the inertial range is a universal constant of turbulence. Considering times $t > \tau_b$, we calculated the average value of the angle across l_0 averaging over both datasets, which gives an estimate of $\langle \theta \rangle = 59.3^\circ$ with an estimated uncertainty of $\pm 2^\circ$ (Fig. 3a).

Using the values that we measured for C_1 and g , and plugging them into eq. (7), we can predict the value of the average angle cosine $\langle \alpha \rangle_{th} = 0.422 \pm 0.042$ (the uncertainty reflect uncertainty in the values of C_1 and g). Furthermore, using the direct empirical measurement, we calculate that $\langle \alpha \rangle_{meas} = 0.46 \pm 0.03$ (here the uncertainty reflects the slight variance in the experimental and numerical estimates). Evidently, these two independent measurements are in good agreement given the 10% accuracy of the first order approximation we used. This confirms eq. (7) for the available degree of uncertainty.

In contrast to the behavior in the inertial range, Fig. 3b shows the evolution of $\langle \theta \rangle$ for pairs outside the inertial range, with $l_0 > L$ using the DNS data. Particles with such a large value of the initial separation are in the diffusive, Taylor range of turbulent pair dispersion, since velocity fluctuations are no longer correlated at these scales⁴. As for the inertial range case (Fig. 3a), $\langle \theta \rangle$ is initially close to 90° and decreases rapidly. However, unlike in the inertial range case, here the curves do not plateau; instead, they reach local minima with values that depend on l_0 , and then increase with time. This behavior of $\langle \theta \rangle$ agrees with the prediction for the trend of $\langle \theta \rangle \rightarrow 90^\circ$ for diffusing particles (second scenario in Sec. 2.1). Overall, our observations confirm that in turbulence, only pairs in the super-diffusive pair dispersion regime manifest the plateau of average pair dispersion angle.

Discussion

Our work offers a framework which reveals the universality of turbulent pair dispersion. We show that the angle between the separation and the relative velocity vectors of separating particles is biased towards oblique values, and the evolution of its average, $\langle \theta \rangle$, follows three distinct regimes in homogeneous isotropic turbulence. Starting from an unbiased value of approximately 90° , $\langle \theta \rangle$ decreases linearly during the initial ballistic regime, while in the diffusive regime $\langle \theta \rangle$ increases back towards the unbiased value of 90° . Yet, the key discovery of our work is that in the inertial range of turbulence $\langle \theta \rangle$ plateaus at a constant value of approximately 59° independently of the initial conditions and of the dissipation rate, making $\langle \theta \rangle$ a universal constant of turbulence.

In Section 2.1, we employed Richardson's classical theory⁸ to estimate the mean value of α (namely, $\cos \theta$) analytically, arriving at eq. (7). Nevertheless, the validity of Richardson's law with the unique t^3 scaling is observed only for small initial separations or separation velocities^{10,15-17,21,22}, while our work establishes that the constancy of $\langle \theta \rangle$ holds throughout the entire inertial range (Fig. 3). To confirm the validity of the estimate provided by Eq. (7), we measured the Richardson constant, g , using particles with initial separations in the range in which Richardson's theory holds. In this sense, Eq. (7) can be understood as a relation that matches the values of g and the new universal alignment property in the limited range where the validity of both overlap. Further theoretical treatment is still needed to fully understand the alignment property.

Determining the time scaling of the separation between particles in the inertial range is one of the long-standing open problems in turbulence. In particular, it is not yet clear whether the elusiveness of empirically confirming Richardson's Eq. (6) is due to a failure of the assumption of the theory itself (i.e. a scale dependent diffusivity)^{30–33} or whether they are due to issues in the measurements. Namely, had the Reynolds numbers in measurements been higher and the duration of measurements been longer, would Richardson's classical predictions be recovered then? Unlike direct scaling measurements, our work shows that the inertial range behavior of $\langle\theta\rangle$ is clearly observed at the Reynolds numbers and measurement durations readily available with current technological capabilities. In particular, the inertial range behavior is robustly observed for particle pairs with l_0 values throughout the whole inertial range (Fig. 3a). A central difference between $\langle\theta\rangle$ and the direct scaling method is that while θ depends on instantaneous regulation of the separation process by the flow (namely on alignment properties of the separation velocity), the scaling exponents integrate it in time and thus can accumulate deviations. Therefore, while our observation that $\langle\theta\rangle$ is constant in the inertial range suggests that the internal regulation of the flow leading to Richardson's law exists in realistic, terrestrial turbulence, whether this leads to converged scaling exponents in a finite Reynolds number flow is still debated²².

An important outcome of our work is that it opens the opportunity for verifying the three regimes of turbulent pair dispersion in future measurements. In particular, measuring the evolution of $\langle\theta\rangle$ instead of the separation scaling exponents is advantageous because of three main reasons. First, confirming the super diffusive regime using $\langle\theta\rangle$ amounts to measuring a constant value, which, due to the finite nature of measurements, is much easier than measuring scaling regimes with high exponents. Second, θ is inherently scale-invariant, so the complications that arise due to the intermittency of pair dispersion and initial separation dependence are avoided. Third, the plateau of $\langle\theta\rangle$ appears early after the ballistic regime (for $t \geq 0.5\tau_b$, Fig. 3), so it is not necessary to obtain very long particle trajectories. Indeed, the plateau of $\langle\theta\rangle$ is detected for all initial separations inside the inertial range ($l_0 < L$). Therefore, our framework allows confirming the effects of turbulence on scalar dispersion over a wide range of flows and under realistic conditions - a crucial step both for our understanding of turbulent flows and for modeling dispersion.

To conclude, our geometrical framework opens a new perspective in turbulent dispersion research since its universality allows characterizing pair dispersion in a wide range of turbulent flows. Even under conditions that depart from the ideal ones considered here (i.e., quasi-homogeneous and isotropic), observing at which times and initial separations $\langle\theta\rangle$ remain at a constant value allows to quantitatively assert the range of scales in which the inertial range manifests, a particularly crucial issue for environmental flows^{34–36}. Therefore, the framework we propose can be used to characterize a large variety of dispersion processes in nature. For example, going back to the question of how fast particles mix in the ocean, measuring $\langle\theta\rangle$ in field experiments will allow determining at which scales isotropic turbulence phenomenology drives dispersion and under which of the three regimes, thus enabling more accurate dispersion estimations of algae blooms, plastic debris and oil spills in the ocean.

Methods

Empirical dataset

Our work uses two independent empirical datasets to confirm our analysis - the results of a numerical simulation, and the results of a particle tracking experiment.

Direct numerical simulation. We used the results of a Direct numerical Simulation of the Navier-Stokes equation with a large scale, statistically stationary and homogeneous forcing. The simulation was performed, and its results are stored and maintained, by the team of the Johns Hopkins Turbulence Database²⁵ (JHTDB). The results of the simulation are stored as Eulerian fields, holding data for a time duration of approximately 5 integral timescales over a periodic cubical domain with 1024^3 nodes; the Taylor microscale Reynolds number is $Re_\lambda \approx 433$. Since its publication, the JHTDB had become a gold standard and an hypothesis testing tool in the turbulence community.

To study pair dispersion using the results of the JHTDB simulation we calculated trajectories of flow tracers by time integration of the velocity field. For that, we used JHTDB's `#get_position#` function, following the results of²⁶. Overall, we integrated approximately 12,500 trajectories, each over a time span of three integral timescales. Trajectories were integrated in 63 groups starting from random initial positions and times in the computational domain. By pairing initially close trajectories with one another we obtained a dataset that holds $\sim 6 \times 10^5$ pairs of trajectories with initial separation inside the inertial range (namely, with $l_0 \lesssim 200\eta$), and approximately 10^6 trajectory pairs with initial separations larger than that. Fig. 1 shows a 3D rendering of one such group of trajectories.

In addition to the Lagrangian trajectories, we also downloaded Eulerian velocity samples over a regularly spaced grid. This dataset was used to calculate the first-order absolute structure function (Fig. 2b). For this purpose we used samples distributed over three orthogonal planes in the computational domain, taken at evenly spaced intervals over time and space, using approximately 6η of separation in space and one half integral time scale in time.

3D particle tracking experiment. We used an experimental dataset obtained from a 3D Particle Tracking Velocimetry (3D-PTV) experiment. The turbulent flow was generated inside an octagonal cylindrical tank that is constructed of an aluminum frame fitted with eight transparent glass windows (Fig. 2a). The tank was filled with approximately 17.5 liters of de-ionized filtered water. Turbulent flow was generated in the tank using eight 45 W DC servo-motors, each connected to a vertical shaft that is fitted with a pair of propellers. Each motor was operated individually using a random actuator that alters the direction of rotation at random time intervals taken from a Poisson distribution with an average of 0.1 s, in a setup similar to those used in refs. 21, 37.

The flow was measured using 3D Particle Tracking Velocimetry (3D-PTV)²⁷. The water was seeded with $70\mu\text{m}$ fluorescent tracer particles of density $\rho = 1030 \text{ kg m}^{-3}$. The particles were then illuminated by an expanded laser beam (537 nm), that was masked to illuminate a prismatic rectangular volume at the center of the tank. Four high-speed digital cameras (Microtron, 1280×1024 pixels) were synchronized and operated at 500 Hz to record images of the tracer particles as they were carried by the flow. The cameras were calibrated using the self-calibration method³⁸ using a calibration target on which 438 points were marked at known locations over three parallel planes. The setup yielded a static calibration uncertainty of approximately $50 \mu\text{m}$ based on the root mean squared calibration error. In addition, the cameras were fitted with high pass optical filters to better visualize the fluorescent particles.

The tracer images were analysed following the 3D-PTV methodology by using our open-source software MyPTV²⁸ that is freely available online. The trajectories were then smoothed using a moving third-order polynomial spline with a window size of 11 samples, and 5 samples at the edge of each trajectory were discarded. We analysed 20 s of data in total, which is on the order of 100 integral timescales of the flow. Our measurement spanned a measurement volume of $70 \times 70 \times 40 \text{ mm}$, where each of the 10,000 frames in our post-

processed dataset contained approximately $\sim \mathcal{O}(10^3)$ particles. The root mean square of the velocity fluctuations was $u' = 58 \text{ mm s}^{-1}$, the integral length scale was $L = 20.5 \text{ mm}$, the dissipation rate was $\epsilon = \frac{1}{2} \frac{u'^3}{L} = 4950 \text{ mm}^2 \text{ s}^{-3}$; correspondingly, $\eta = 0.12 \text{ mm}$, and the Taylor microscale and Reynolds number are $\lambda = \sqrt{15} \frac{u'}{\epsilon} = 3.1 \text{ mm}$, $\text{Re}_\lambda = \frac{u' \lambda}{\nu} \approx 188$ (see supplementary materials for details on these calculations). A 3D rendered animation of trajectories from our experiment is shown in Supplementary Video 2. The full data set of approximately $\sim \mathcal{O}(6 \times 10^5)$ trajectories can be downloaded in ref. 29.

Calculation of the coefficient b

In equation (5), we calculated the first moment of particle separations, l , using theoretical predictions of its PDF and its second moment. In particular, two shapes of the PDF of l were predicted assuming diffusive separation from a point source⁶. The first was obtained by Richardson⁸

$$q_R(l) = \frac{a_{R,1}}{(\pi \langle l^2 \rangle)^{3/2}} \cdot \exp \left[-a_{R,2} \left(\frac{l^2}{\langle l^2 \rangle} \right)^{1/3} \right], \tag{10}$$

where $a_{R,1} = \frac{429}{70} \sqrt{\frac{143}{2}}$ and $a_{R,2} = \left(\frac{1287}{8}\right)^{1/3}$, and the second was obtained by Batchelor⁴

$$q_B = \left(\frac{3}{2\pi \langle l^2 \rangle} \right)^{3/2} \exp \left(-\frac{3}{2} \frac{l^2}{\langle l^2 \rangle} \right). \tag{11}$$

In both cases the second moment $\langle l^2 \rangle$ appears explicitly in the expressions, which means that the n^{th} moment can be expressed as $\langle l^n \rangle \propto \langle l^2 \rangle^{n/2}$. In particular, for both PDFs, the n^{th} moment is readily calculated by solving

$$\langle l^n \rangle = \int_0^\infty l^n q(l) 4\pi l^2 dl \tag{12}$$

using the following formula³⁹

$$\int_0^\infty x^n \exp(-ax^k) dx = \frac{1}{k} a^{-\frac{(n+1)}{k}} \Gamma \left(\frac{n+1}{k} \right) \tag{13}$$

where $\Gamma(x)$ is the Gamma function. Thus, for the Richardson PDF, $q_R(l)$, we obtain $b = \frac{6a_{R,1}}{\sqrt{\pi} a_{R,2}^6} \Gamma(6) \approx 0.813$, whereas for the Batchelor PDF, $q_B(l)$, we obtain $b = \sqrt{\frac{27}{2\pi}} \left(\frac{2}{3}\right)^2 \Gamma(2) \approx 0.921$. These calculations result in the following range of $b = 0.867 \pm 0.054$. Notably, from the empirical point of view, the measured distribution of l may have a different shape, so q_R and q_B are considered as two limit cases^{10,13} reflected in the uncertainty range of b ; in accordance, direct estimation of b using our empirical datasets gives $b \approx 0.84$, in agreement with the calculations.

The mixed Eulerian-Lagrangian structure function

We here derive the mixed-Eulerian-Lagrangian first order absolute structure function. For that, we consider an ensemble of pairs of Lagrangian particles that are initially separated by a distance l_0 . The particles are free to move, so the distance between each of the pairs in the ensemble changes as a function of time. Thus, the first order structure function is obtained from the ensemble

average as

$$\langle |\Delta \mathbf{v}| \rangle = \iint |\Delta \mathbf{v}| \mathcal{P}(|\Delta \mathbf{v}|, l) dl d|\Delta \mathbf{v}| \tag{14}$$

where $\mathcal{P}(|\Delta \mathbf{v}|, l)$ is the joint PDF for the absolute value of the pairwise relative velocity and the distance (see ref. 4, Sec. 24.2). Using Bayes' theorem⁴⁰, the join PDF is written using the marginal and the conditional PDF of the distances and the relative velocity respectively $\mathcal{P}(|\Delta \mathbf{v}|, l) = \mathcal{P}(|\Delta \mathbf{v}| | l) \cdot q(l) 4\pi l^2$, where as in Section 4.2, $q(l)$ is the PDF for the distance l . We first solve the integral over the relative velocities and obtain

$$\int \left[\int |\Delta \mathbf{v}| \mathcal{P}(|\Delta \mathbf{v}| | l) d|\Delta \mathbf{v}| \right] q(l) 4\pi l^2 dl = \int C_1 \epsilon^{1/3} l^{1/3} q(l) 4\pi l^2 dl \tag{15}$$

where we have used the fact the the average of $|\Delta \mathbf{v}|$ at a given scale l is the purely Eulerian first order structure function, while employing Kolmogorov's universal similarity theory²⁴ for l in the inertial range; this is justified because the initial position of each pair is chosen randomly over space and time, and because of the l_0 independence in the inertial range. Following that, we solve the integral over the particle distances while employing both Richardson's and Batchelor's PDFs, $q_R(l)$ and $q_B(l)$. In both cases, we obtain the solution in the form

$$\langle |\Delta \mathbf{v}| \rangle = c C_1 \left(\epsilon \sqrt{\langle l^2 \rangle} \right)^{1/3} \tag{16}$$

where c is a constant that depends on the shape of $q(l)$ that was chosen, being equal to 0.952 for the Batchelor PDF, and 0.885 for the Richardson PDF. Thus, we will use the value $c = 0.918 \pm 0.034$ where the uncertainty is taken to make sure we are covering the two possible shapes of the PDF.

A Taylor series expansion for $\langle \alpha \rangle$ in the inertial range

For ease of notation, we denote $X \equiv |\Delta \mathbf{v}|$ and $Y \equiv \frac{dl}{dt}$. To obtain eq. (5), we write $\alpha(X, Y) = \frac{1}{X} Y$, and Taylor expand it around the averages $\langle X \rangle$ and $\langle Y \rangle$. After averaging the result, we obtain⁴¹

$$\begin{aligned} \langle \alpha \rangle &= \alpha_0 + \alpha_1 + \alpha_2 + \dots \\ \alpha_0 &= \alpha|_{\langle X \rangle, \langle Y \rangle} = \frac{1}{\langle X \rangle} \langle Y \rangle \\ \alpha_1 &= \frac{\partial \alpha}{\partial X} |_{\langle X \rangle, \langle Y \rangle} \langle X - \langle X \rangle \rangle + \frac{\partial \alpha}{\partial Y} |_{\langle X \rangle, \langle Y \rangle} \langle Y - \langle Y \rangle \rangle = 0 \\ &\vdots \\ \alpha_n &= \left\langle \frac{1}{n!} \left[\sum_{k=0}^n \binom{n}{k} \frac{\partial^{n-k}}{\partial X^{n-k}} \frac{\partial^k \alpha}{\partial Y^k} |_{\langle X \rangle, \langle Y \rangle} (X - \langle X \rangle)^{n-k} (Y - \langle Y \rangle)^k \right] \right\rangle \end{aligned} \tag{17}$$

Let us note that the values of α and its derivatives estimated at $\langle X \rangle$ and $\langle Y \rangle$ are constants that multiply mixed central moments of X and Y .

Data availability

The experimental dataset generated and analyzed during the current study is available in "Zenodo" with the identifier <https://doi.org/10.5281/zenodo.6802679>. Numerical data from the DNS dataset used in this study can be downloaded from the Johns Hopkins Turbulence Database at <http://turbulence.pha.jhu.edu/>. Other data used to support the finding of this study are available from the authors upon reasonable request.

Code availability

The code used to obtain the numerical DNS dataset is available at the supplementary information file.

References

- Batchelor, G. K. Diffusion in a field of homogeneous turbulence: II. The relative motion of particles. *Math. Proc. Camb. Philos. Soc.* **48**, 345–362 (1952).
- Edouard, S., Legras, B., Lefevre, F. & Eymard, R. The effect of small-scale inhomogeneities on ozone depletion in the Arctic. *Nature* **384**, 444–447 (1996).
- Griffa, A. et al. Investigating transport pathways in the ocean. *Deep Sea Res. Part II: Topical Stud. Oceanogr.* **85**, 81–95 (2013).
- Monin, A. S., Yaglom, A. M. *Statistical Fluid Mechanics*. Dover Publications inc., Mineola, N.Y. (1972). <https://doi.org/10.1119/1.10870>
- Sawford, B. Turbulent relative dispersion. *Annu. Rev. Fluid Mech.* **33**, 289–317 (2001).
- Salazar, J. P. L. C. & Collins, L. R. Two-particle dispersion in isotropic turbulent flows. *Annu. Rev. Fluid Mech.* **41**, 405–432 (2009).
- Taylor, G. I. Diffusion by continuous movements. *Proceedings of the London Mathematical Society* (1921). <https://doi.org/10.1112/plms/s2-20.1.196>
- Richardson, L. F. Atmospheric diffusion shown on a distance-neighbour graph. *Proc. R. Soc. Lond. Ser. A, Containing Pap. A Math. Phys. Character* **110**, 709–737 (1926).
- Yeung, P. K. Direct numerical simulation of two-particle relative diffusion in isotropic turbulence. *Phys. Fluids* **6**, 3416–3428 (1994).
- Ott, S. & Mann, J. An experimental investigation of the relative diffusion of particle pairs in three-dimensional turbulent flow. *J. Fluid Mech.* **422**, 207–223 (2000).
- Biferale, L. et al. Lagrangian statistics of particle pairs in homogeneous isotropic turbulence. *Phys. Fluids* **17**, 115101 (2005).
- Bourgoin, M., Ouellette, N. T., Xu, H., Berg, J. & Bodenschatz, E. The role of pair dispersion in turbulent flow. *Science* **311**, 835–838 (2006).
- Ouellette, N. T., Xu, H., Bourgoin, M., Bodenschatz, E. An experimental study of turbulent relative dispersion models. *N. J. Phys.* **8** <https://doi.org/10.1088/1367-2630/8/6/109> (2006).
- Buaría, D., Sawford, B. L. & Yeung, P. K. Characteristics of backward and forward two-particle relative dispersion in turbulence at different Reynolds numbers. *Phys. Fluids* **27**, 105101 (2015).
- Shnapp, R. & Liberzon, A. Generalization of turbulent pair dispersion to large initial separations. *Phys. Rev. Lett.* **120**, 244502 (2018).
- Tan, S. & Ni, R. Universality and intermittency of pair dispersion in turbulence. *Phys. Rev. Lett.* **128**, 114502 (2022).
- Elsinga, G. E., Ishihara, T. & Hunt, J. C. R. Non-local dispersion and the reassessment of Richardson's t^3 -scaling law. *J. Fluid Mech.* **932**, 17 (2022).
- Boffetta, G., Sokolov, I. M. Relative dispersion in fully developed turbulence: the Richardson's law and intermittency corrections. *Phys. Rev. Lett.* **88** <https://doi.org/10.1103/PhysRevLett.88.094501> (2002).
- Yeung, P. K. & Borgas, M. S. Relative dispersion in isotropic turbulence. Part 1. Direct numerical simulations and Reynolds-number dependence. *J. Fluid Mech.* **503**, 93–124 (2004).
- Scatamacchia, R., Biferale, L. & Toschi, F. Extreme events in the dispersions of two neighboring particles under the influence of fluid turbulence. *Phys. Rev. Lett.* **109**, 144501 (2012).
- Berg, J., Lüthi, B., Mann, J. & Ott, S. Backwards and forwards relative dispersion in turbulent flow: An experimental investigation. *Phys. Rev. E* **74**, 016304 (2006).
- Kishi, T., Matsumoto, T. & Toh, S. Two-time Lagrangian velocity correlation function for particle pairs in two-dimensional inverse energy-cascade turbulence. *Phys. Rev. Fluids* **7**, 064604 (2022).
- Tsinober, A. *An Informal Conceptual Introduction to Turbulence*. Springer https://doi.org/10.1007/978-90-481-3174-7_6 (2009).
- Kolmogorov, A. N. The local structure of turbulence in incompressible viscous fluid for very large Reynolds numbers. *Cr Acad. Sci. URSS* **30**, 301–305 (1941).
- Li, Y. et al. A public turbulence database cluster and applications to study Lagrangian evolution of velocity increments in turbulence. *J. Turbulence* (9), **31** <https://doi.org/10.1080/14685240802376389> (2008).
- Yu, H. et al. Studying Lagrangian dynamics of turbulence using on-demand fluid particle tracking in a public turbulence database. *J. Turbulence* (13), **12** (2012).
- Dracos, T. *Three-dimensional velocity and vorticity measuring and image analysis technique: Lecture notes from the short course held in Zurich, Switzerland*. Springer (1996). <https://www.springer.com/gp/book/9780792342564>
- Shnapp, R. MyPTV: A Python package for 3D particle tracking. *J. Open Source Softw.* **7**, 4398 (2022).
- Shnapp, R., Brizzolara, S., Neamtu Halic, M., Gambino, A., Holzner, M. Lagrangian particles in turbulence: an experimental data set. *Zenodo* <https://doi.org/10.5281/zenodo.6802680> (2022).
- Bitane, R., Homann, H. & Bec, J. Time scales of turbulent relative dispersion. *Phys. Rev. E* **86**, 045302 (2012).
- Sokolov, I. M., Klafter, J. & Blumen, A. Ballistic versus diffusive pair dispersion in the Richardson regime. *Phys. Rev. E* **61**, 2717–2722 (2000).
- Thalabard, S., Krstulovic, G. & Bec, J. Turbulent pair dispersion as a continuous-time random walk. *J. Fluid Mech.* **755**, 4 (2014).
- Bourgoin, M. Turbulent pair dispersion as a ballistic cascade phenomenon. *J. Fluid Mech.* **772**, 678–704 (2015).
- Celani, A., Cencini, M., Vergassola, M., Villermaux, E. & Vincenzi, D. Shear effects on passive scalar spectra. *J. Fluid Mech.* **523**, 99–108 (2005).
- Pitton, E., Marchioli, C., Lavezzo, V., Soldati, A. & Toschi, F. Anisotropy in pair dispersion of inertial particles in turbulent channel flow. *Phys. Fluids* **24**, 073305 (2012).
- Polanco, J. I., Vinkovic, I., Stelzenmuller, N., Mordant, N. & Bourgoin, M. Relative dispersion of particle pairs in turbulent channel flow. *Int. J. Heat. Fluid Flow.* **71**, 231–245 (2018).
- Lüthi, B., Ott, S., Berg, J. & Mann, J. Lagrangian multi-particle statistics. *J. Turbulence* **8**, N45 (2007).
- Mass, H. G., Gruen, D. & Papantoniou, D. Particle tracking velocimetry in three-dimensional flows part i: Photogrammetric determination of particle coordinates. *Exp. Fluid* **15**, 133–146 (1993).
- Gradshteyn, I. S., Ryzhik, I. M. *Table of Integrals, Series, and Products*, 7th edn. Academic Press <https://doi.org/10.1016/C2010-0-64839-5> (2007).
- Van Kampen, N. G. *Stochastic Processes in Physics and Chemistry*. Elsevier <https://doi.org/10.1016/B978-0-444-52965-7.X5000-4> (2007).
- Benaroya, H., Han, S. M., Nagurka, M. *Probability Models in Engineering and Science* vol. 192. CRC press (2005).

Acknowledgements

We would like to thank Prof. Guido Boffetta and Dr. Simone Boi for helpful comments and discussions. R.S. is a Rothschild fellow. M.H. and S.B. acknowledge financial support from the DFG priority program SPP 1881 Turbulent Superstructures under Grant No. HO5519/1-2.

Author contributions

R.S. initiated the study. The theory was developed by R.S., S.B., M.M.N.H., A.G. and M.H. The numerical data was obtained and analyzed by R.S. The experiment was designed and performed, and its results were analyzed by R.S., S.B., M.M.N.H. and A.G. The paper was written by R.S., S.B., M.M.N.H., A.G., and M.H.

Competing interests

The authors declare no competing interests.

Additional information

Supplementary information The online version contains supplementary material available at <https://doi.org/10.1038/s41467-023-39903-6>.

Correspondence and requests for materials should be addressed to Ron Shnapp.

Peer review information *Nature Communications* thanks the anonymous, reviewer(s) for their contribution to the peer review of this work.

Reprints and permissions information is available at <http://www.nature.com/reprints>

Publisher's note Springer Nature remains neutral with regard to jurisdictional claims in published maps and institutional affiliations.

Open Access This article is licensed under a Creative Commons Attribution 4.0 International License, which permits use, sharing, adaptation, distribution and reproduction in any medium or format, as long as you give appropriate credit to the original author(s) and the source, provide a link to the Creative Commons license, and indicate if changes were made. The images or other third party material in this article are included in the article's Creative Commons license, unless indicated otherwise in a credit line to the material. If material is not included in the article's Creative Commons license and your intended use is not permitted by statutory regulation or exceeds the permitted use, you will need to obtain permission directly from the copyright holder. To view a copy of this license, visit <http://creativecommons.org/licenses/by/4.0/>.

© The Author(s) 2023